Journal of Magnetic Resonance 242 (2014) 197–202

Contents lists available at ScienceDirect

Journal of Magnetic Resonance

journal homepage: www.elsevier.com/locate/jmr

Chirped CPMG for well-logging NMR applications

Leah B. Casabianca [a], Daniel Mohr [a], Soumyajit Mandal [b], Yi-Qiao Song [b], Lucio Frydman [a,*]

[a] Department of Chemical Physics, The Weizmann Institute of Science, Rehovot 76100, Israel
[b] Schlumberger-Doll Research, 1 Hampshire Street, Cambridge, MA 02139, United States

ARTICLE INFO

Article history:
Received 29 December 2013
Revised 27 February 2014
Available online 12 March 2014

Keywords:
Well-logging NMR
Chirped pulses
CPMG
Sensitivity enhancement
Ex situ NMR

ABSTRACT

In NMR well-logging, the measurement apparatus typically consists of a permanent magnet which is inserted into a bore, and the sample is the rock surrounding the borehole. When compared to the conditions of standard NMR experiments, this application is thus challenged by relatively weak and invariably inhomogeneous B_0 and B_1 fields. Chemical shift information is not generally obtained in these measurements. Instead, diffusivity, porosity and permeability information is collected from multi-echo decay measurements – most often using a Carr–Purcell Meiboom–Gill (CPMG) pulse sequence to enhance the experiment's limited sensitivity. In this work, we explore the consequences of replacing the hard square pulses used in a typical CPMG sequence with chirped pulses sweeping a range of frequencies. The greater bandwidths that for a maximum B_1 level can be excited by chirped pulses translates into marked expansion of the detection volume, and thus significant signal-to-noise improvements when compared to standard CPMG acquisitions using hard pulses. This improvement, usually amounting to signal enhancements $\geqslant 3$, can be used to reduce the experimental time of NMR well-logging measurements, for measuring T_2 even when B_0 and B_1 inhomogenieties complicate the measurements, and opening new opportunities in the determination of diffusional properties.

1. Introduction

NMR has become an integral tool in well-logging applications. In contrast to the typical laboratory NMR experiment where the sample rests inside the magnet, in NMR well-logging the apparatus – including a permanent magnet – is inserted into the well bore and the sample is actually the rock surrounding the borehole [1,2]. Both the B_0 and B_1 fields are projected outward from the well-logging apparatus into the surrounding environment, enabling the sample's *ex situ* characterization by NMR. As a result of this "inside-out" procedure, relatively weak magnetic fields as well as strong inhomogeneities in both B_0 and B_1 fields are typical features of these experiments [3]. These factors combined imply that no meaningful chemical shift information can be obtained from this kind of experiment [1]; instead, the fluid properties and the characteristics of the porous materials (e.g. porosity and permeability) are extracted from diffusion and spin relaxation (T_1 and T_2) measurements [4]. A common approach for enhancing the sensitivity of all these low-field measurements, as well as for T_2 determinations, is the Carr–Purcell Meiboom–Gill (CPMG) sequence [5,6]. CPMG involves a single excitation pulse followed by a series of phase-shifted π pulses, leading to an echo train of signals whose digitization has proven useful for enhancing the sensitivity of inhomogeneously-broadened lines.

Within a well-logging setting, CPMG faces dual challenges stemming from the inhomogeneity of the B_1 used and from the power limitations that can be imparted onto the B_1. These will limit in turn the bandwidths of the spins that are excited, and which can be subsequently refocused by the pulses. Similar challenges arise in the field of CPMG acquisitions in inhomogeneously broadened solids; in this area, Bhattacharyya and Frydman [7] showed that frequency-swept pulses can be used in a spin-echo experiment to excite a broad range of frequencies, and enhance for a given maximal B_1 field the range of excitable offsets by nearly fourfold factors. In those wideline quadrupolar solid state NMR experiments, distortion-free powder patterns were demonstrated by two means. The first included setting the sweep rate of the refocusing pulse equal to twice that of the excitation pulse, $R_{ref} = 2R_{exc}$. As shown by Bodenhausen et al. this causes all crystallites to be refocused at the same time [8,9], leading to full echoes akin to that formed by a Hahn sequence based on hard pulses – but enjoying the benefits of the broader bandwidth and immunity to inhomogeneities afforded by the radiofrequency (RF) sweep. A second way assayed to extract an undistorted powder pattern from a broad line used chirped pulses whose sweep rates were set as $R_{ref} = R_{exc}$. This caused all

* Corresponding author. Fax: +972 8 9344123.
E-mail address: lucio.frydman@weizmann.ac.il (L. Frydman).

http://dx.doi.org/10.1016/j.jmr.2014.02.025
1090-7807/

isochromats to be refocused at different times as determined by their resonance frequencies. In this case frequency-dependent echoes were formed, from which spectra could be extracted by taking the absolute value – without a need for Fourier transformation. Further expansions of these concepts to increase the sensitivity enhancement of solid-state NMR in a variety of spin-1/2 and spin > ½ systems, have also been discussed [10,11].

In this work, we explore the potential of these frequency-swept (chirped-)CPMG experiments to increase the signal-to-noise ratio (SNR), in *ex situ* NMR setups of the kind found in well-logging experiments. In the next section, we briefly review how a swept excitation followed by a series of frequency-swept refocusing pulses leads to echo trains with alternating free-induction-decay (FID) signals resembling those of a conventional CPMG train ("FID" echoes), interleaved with time-domain echoes resembling the actual NMR spectrum ("spectral" echoes). The next section also justifies the use of frequency-swept pulses as a sensitivity-enhancement tool in scenarios that, as happens in well-logging NMR, have to face large inhomogeneous line widths as well as limited capabilities in terms of the available RF peak powers. With these theoretical considerations at hand we then present results from two different NMR setups that validate the theoretical SNR gain expectations, and rationalize these in terms of the excitation bandwidths that are achieved by these sequences. We conclude with a brief discussion on the opportunities opened up by these new sequences.

2. Chirped-CPMG: Principles and advantages

2.1. "FID" and "spectral" echoes

To derive the conditions needed to retrieve the FID- and spectral-echoes just alluded to, we follow the formalism described in Refs. [7,12] to compute how chirped RF pulses will sequentially excite and refocus different frequency isochromats at different times. In these cases, as in the sequences to be considered here, spins are assumed excited by a RF pulse whose offset is linearly swept between O_i and O_f over a time interval τ_{exc} with a constant sweep rate $R_{exc} = (O_f - O_i)/\tau_{exc}$. For simplicity we will also assume that the sweep is symmetric about the single-peak's on-resonance frequency; i.e., that $O_i = -O_f$. The overall phase accumulated by the spins at the end of the initial excitation pulse will then be given by a sum of two terms: one representing the phase accrued by the RF at a time $\tau(f)$ when the sweep reaches the isochromat's resonance frequency offset f, and another that accounts for the phase accrued by the spins in this isochromat due to their free precession during the remainder of the excitation pulse. Taking these two terms into account leads to an overall frequency-dependent excitation phase:

$$\phi_{exc}(f) = \phi_{RF}[\tau(f)] + [\tau_{exc} - \tau(f)] \cdot f = \left(\frac{O_i}{R_{exc}} + \tau_{exc}\right) f - \frac{f^2}{2R_{exc}}, \quad (1)$$

On the other hand, the phase imparted to the evolving spins by a refocusing pulse characterized by a rate R_{ref} and length τ_{ref} covering the same $O_i \to O_f$ range, is given by [12]:

$$\phi_{ref}(f) = -\tau(f) f + 2\phi_{RF}[\tau(f)] + [\tau_{ref} - \tau(f)] \cdot f = \frac{(O_i + O_f)}{R_{ref}} f - \frac{f^2}{R_{ref}}. \quad (2)$$

In a spin echo sequence as diagrammed in Fig. 1a, with an excitation pulse followed by a refocusing pulse after a time τ_δ, the total overall phase of the spins as a function of the acquisition time t will therefore be given by:

$$\Phi_{acquisition}(f, t) = f^2 \left(\frac{1}{2R_{exc}} - \frac{1}{R_{ref}}\right) - f\left(\frac{O_f}{R_{exc}} + \tau_\delta\right) + f \cdot t. \quad (3)$$

Setting $R_{ref} = 2R_{exc}$ the quadratic term in Eq. (3) disappears, and an echo forms for all isochromats at a time $\tau_{echo} = \tau_\delta + \frac{O_f}{R_{exc}} = \tau_\delta + \frac{\tau_{exc}}{2}$. By contrast, if $R_{ref} \neq 2R_{exc}$, each isochromat will refocus at a different time depending on its own frequency. The refocusing time will be given by the stationary phase condition $\frac{d}{df}[\Phi_{total}(f)]_{f=f_t} = 0$; as shown in Refs. [7,12], this leads to an observable signal:

$$S(t) \propto e^{i\Phi_{total}(f_t)} \cdot \sqrt{\frac{2\pi}{\left|\frac{d^2\Phi_{total}}{df^2}\right|_{f=f_t}}} \cdot I(f_t), \quad (4)$$

where $I(f)$ is the frequency domain spectrum arising from the field inhomogeneity. Due to the linear relationship between f_t and t that follows from the application of a linear chirp pulse, the NMR spectrum $I(f)$ will then be proportional to $S(t)$ in a point-by-point fashion. Thus the NMR spectrum can be retrieved from this echo by simply taking the absolute value of the FID signal $|S(t)|$, without the need for a Fourier transform.

The above analysis describes what happens when single chirp excitation and refocusing pulses are used to achieve a single spin-echo. For the CPMG-like sequences used in well-logging applications, this analysis needs to be expanded to explore what happens when additional refocusing pulses are added. Fig. 1b exemplifies this, with an additional refocusing pulse concatenated to the sequence of Fig. 1a under the assumption of $R_{ref} = 2R_{exc}$. As mentioned earlier, an echo will form under this condition after the application of the first refocusing pulse at a time $\tau_\delta + \tau_{exc}/2$; in order to center this echo, we set the acquisition time during which signals were collected to run up to $T_{acq} = \tau_{exc} + 2\tau_\delta$. At this time the isochromat's phases will be given by $\phi_{End\_1^{st}Echo} = f(\tau_\delta + \frac{\tau_{exc}}{2})$; if at this point a second refocusing pulse is applied under identical conditions as the first one, an additional quadratic phase dependence akin to that in Eq. (2) will be gained:

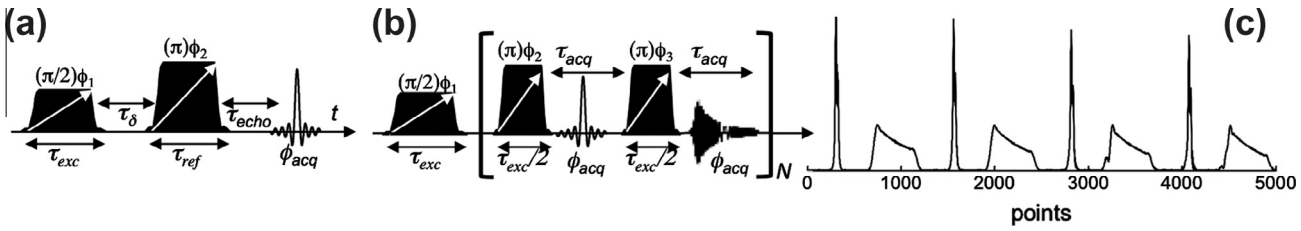

Fig. 1. (a) Frequency-swept spin-echo sequence forming the basis of this study, showing the various timings and definitions. (b) Extension of the single-echo sequence (a) to a chirped-CPMG comprising $2N$ digitized echoes. Given the chosen durations of the π and $\pi/2$ pulses alternating conventional "FID" and f-dependent "spectral" echoes should be generated. (c) Example of the time-domain signal (absolute value) observed upon executing the pulse sequence in (b) on an inhomogeneously broadened sample showing alternating "FID" and "spectral" echoes. In these experiments N was set equal to 4 (leading to 8 echoes) and a suitable pathway selection was ensured by a 4-scan phase cycle $\phi_1 = 90, 270, 180, 0$ $\phi_2 = 0, 0, 90, 90$, $\phi_3 = 90, 90, 0, 0$, $\phi_{acq} = 0, 180, 90, 270$.

$$\Phi_{2^{nd}Echo}(f,t) = -\frac{f^2}{2R_{exc}} + f\left(\tau_\delta + \frac{3\tau_{exc}}{2}\right) - f\cdot t. \quad (5)$$

Frequency-dependent echoes will then form for each isochromat at different times dictated by their particular off-resonance f-value:

$$t_f = -\frac{f}{R_{exc}} + \left(\tau_\delta + \frac{3\tau_{exc}}{2}\right). \quad (6)$$

It follows that if keeping the condition $R_{ref} = 2R_{exc}$ for two post-excitation swept π-pulses, all spin-packets will refocus simultaneously in their first echoes, but at a frequency-dependent time order during their second echo. We refer to the first case a "FID" echo, as it is analogous to the time-domain behavior that results from a typical spin-echo experiment with hard pulses. From it, a frequency-domain spectrum can be extracted by Fourier transformation. By contrast we refer to the second case as to a "spectral" echo, as in this case the spectral profile can be observed directly from a magnitude-mode representation of the time-domain data. This is similar to what happens if a two-pulse chirped spin-echo sequence is executed, under the $R_{ref} \neq 2R_{exc}$ condition. It follows that when additional refocusing pulses are appended to this sequence to form a CPMG-like echo train, subsequent odd-numbered echoes will lead to "FID echoes" while subsequent even-numbered echoes will resemble "spectral echoes". A basic experimental realization of this phenomenon is presented in Fig. 1c. For this experimental FID, 8 echoes were collected with a dwell time of 4.8 μs, 625 points for each echo, sweep bandwidth of 120 kHz, 90° excitation pulse of 3 ms, 180° refocusing pulse of 1.5 ms, and total acquisition time of 36 ms.

2.2. Sensitivity advantages of chirped-CPMG

With these considerations as background, it is worth discussing why and when would it be of interest to depart from hard pulses, and implement CPMG acquisitions using frequency-swept pulses. To this end we shall consider the spectra in well-logging applications to be for all practical purposes "infinitely" broad, in the sense that they span a bigger range of frequency than what can be covered by most pulsed, tuned electronic circuits. The extent of sample that is excited, and with it the sensitivity that will be achieved for a fixed geometry, will thus be given by the bandwidth BW that can be covered by the excitation pulse and by the subsequent refocusing CPMG train. These BWs are in turn given by the excitation pulse τ that is used, according to a fixed time-bandwidth product [13] $BWP = BW\cdot\tau$. As this product is smaller for π than for $\pi/2$ pulses (≈1.1 against 1.5) and τ_π is usually longer than $\tau_{\pi/2}$, the bottleneck limiting the excitation volume in well-logging CPMG acquisitions will usually be given by the CPMG π-pulse portion. For a given maximal $B_1^{\max}$ made available by the hardware, the sample bandwidth available in these hard-pulse experiments will therefore be given by

$$BW_{hard} \approx \frac{BWP}{\tau_\pi} = \frac{BWP\cdot 2\pi\cdot\gamma B_1^{\max}}{\pi}, \quad (7)$$

where we have assumed a pulse angle of π. By contrast, the bandwidths BW that can be excited by a chirped pulse will be generally given by the frequency range $O_f - O_i$ covered during the sweep – regardless of whether involving a $\pi/2$ or a π rotation. While the γB_1 does not directly affect this frequency range, there is in fact a linear relation between the RF fields that are need to impart a small-nutation angle θ_{pulse}, and the square root of the rate $R_{chirp} = (O_f - O_i)/\tau_{chirp}$ at which frequencies are swept [14,15]:

$$\gamma B_1 \approx ChP\cdot\theta_{pulse}\cdot\frac{\sqrt{R_{chirp}}}{2\pi} \quad (8)$$

where ChP is now a "chirp product", ≈1.04 for nutation angles $0 \leqslant \theta_{pulse} < \pi$ (notice that this linear treatment does not include cases involving adiabatic π-based sweeps). Unlike the hard-pulse case, Eq. (8) is not sufficient to constrain an excitation/inversion bandwidth by capping the maximum γB_1 value: for arbitrary $BW_{chirp} = O_f - O_i$ values, it is in principle possible to request a long enough τ_{chirp} to enable Eq. (8)'s fulfillment. At the same time, one would like to make the length of the chirp pulse as short as possible to minimize dissipative losses. It turns out, however, that core assumptions underlying the operation of a chirped pulse – and in particular the sequential addressing of the isochromats that is assumed in Section 2.1 – requires that chirp pulses fulfill minimal time-bandwidth products $TBP_{chirp} = BW_{chirp}\cdot\tau_{chirp} \approx 20$: shorter TBP_{chirp} values will usually lead to behaviors starting to resemble impulse excitations/refocusings. Given a choice for this parameter, BW_{chirp} can be solved for as

$$BW_{chirp} = \frac{2\pi\cdot\gamma B_1^{\max}\sqrt{TBP_{chirp}}}{ChP\cdot\theta_{pulse}} \quad (9)$$

For a CPMG train where the π pulses limit the excitation bandwidth and with it the number of contributing spins, it thus follows that

$$\frac{BW_{chirp}}{BW_{hard}} \approx \frac{\sqrt{TBP_{chirp}}}{ChP\cdot BWP} \quad (10)$$

Whereas as mentioned TBP_{chirp} can be made arbitrarily long, even inserting the "minimum" value of 20 and the above-mentioned figures for ChP and BWP predicts a ratio $\geqslant 4$ for the bandwidths attainable for the same peak powers. Hence, four times as many spins should contribute to a chirped-CPMG train over the number contributing to their hard-pulse counterparts. It is on the basis of this that one can expect a sensitivity enhancement upon utilizing chirped pulses for the execution of well-logging NMR acquisitions.

Before concluding this analysis it is worth noting that this discussion compares SNR increases in the swept-RF over the standard CPMG, assuming that maximum peak power is the sole constraint. We must consider also the increase in average power imparted to the sample when using the chirped-CPMG sequence as compared to the standard CPMG sequence. The power dissipated by a chirped pulse will be given by:

$$power = (\gamma B_1\cdot\Lambda_{env})^2\cdot\tau_{chirp} \quad (11)$$

where Λ_{env} is the envelope of the pulse function; e.g., 0.9 for a WURST-40 pulse. Rearranging Eq. (8), it follows that for a given pulse length, the total power imparted by a chirped pulse is proportional to the chirp bandwidth:

$$power = \left[\frac{ChP\cdot\theta_{pulse}\cdot\Lambda_{env}}{2\pi}\right]^2\cdot BW_{chirp} \quad (12)$$

The power deposited by the frequency-swept pulses will thus increase proportional to the bandwidth. Although the average and total power deposited on a sample are important in clinical and/or preclinical magnetic resonance, depositing higher average and total powers may be of secondary importance in well-logging applications.

3. Experimental methods

The features derived in the preceding section were tested with NMR experiments performed on either a 300/89 Varian VNMRS vertical imaging system (Varian Associates, Inc., Palo Alto, CA, USA), or on a fringe-field scanner at room temperature. For the first setup, ^{1}H NMR spectra were collected at a frequency of 301.973 MHz for a sample of undoped water or water doped with 1 g/L $CuSO_4$ in a 30 mm tube. In order to simulate an inhomogeneous field a

gradient of 4 G/cm was applied parallel to the tube axis throughout the course of the experiment; to further increase the linewidth, the probe and sample were moved away from the sweet spot of the magnet. WURST-40 pulses [16] were used for the chirped pulses. The length of the $\pi/2$ pulses used (τ_{exc}) was 3 ms, and the π pulse (τ_{ref}) used was 1.5 ms; these pulses swept equal frequency ranges, they were clocked every 1 μs, and their amplitudes were set as per Eq. (8). Various sweep bandwidths were used, as listed in Fig. 2. The sweep rates used follow from these bandwidths and from the τ_{exc}, τ_{ref} pulse lengths just mentioned. The delay between the excitation pulse and the first refocusing pulse, τ_δ, was set equal to the minimum allowed by the spectrometer hardware (10 μs). The phase cycling for the standard CPMG sequence was $\phi_1 = 90,270,180,0$, $\phi_2 = 0,0,90,90$ and $\phi_{acq} = 0,180,90,270$; the phase cycling used for the swept-CPMG sequence was as indicated in Fig. 1b. In all experiments acquisitions involved repeating multiple loops N as specified in the captions, with 625 points evenly dwelled in 3 ms long acquisition times digitized in-between the π pulses for each echo.

The fringe-field setup used an un-tuned solenoidal sample coil (ID = 5.5 cm, length = 8.8 cm), custom ultra-broadband transmitter and receiver electronics, and a Kea spectrometer running Prospa version 3.11 software (Magritek, Wellington, New Zealand) for pulse sequence generation and data acquisition. ^{1}H NMR spectra were collected at a frequency of 0.74 MHz in a gradient of 4.7 G/cm. The system provides nearly frequency-independent excitation of the spins with ^{1}H RF nutation fields in the 5–20 kHz range [17,18]. The sample consisted of water doped with $NiCl_2$ ($T_2 \approx 110$ ms), inserted in a cylindrical glass bottle 5 cm in length and in diameter. WURST-40 pulses [16] were used for the chirped pulses, whose length was set to 1.64 and 0.82 ms for the $\pi/2$ and π chirped pulses, respectively. For the hard-pulse CPMG version, $\pi/2$ and π pulses were set to 50 and 100 μs, respectively.

4. Results

Fig. 2 illustrates the increased bandwidth that can be excited using a frequency-swept CPMG pulse sequence, when compared to what is addressed by a standard CPMG operating at the same maximum power levels. This figure shows the frequency domain spectra obtained from chirped and from square-pulse CPMG experiments collected at several γB_1 RF field strengths. The sample was ^{1}H from water positioned in a 30-mm NMR tube inserted in a vertical NMR magnet, whose field homogeneity was spoiled by applying a gradient in the z-direction during acquisition and by moving the sample and probe out of the sweet spot of the magnet. This lead to a broad line with a spectral shape as seen in Fig. 2. For the chirped-CPMG experiments, "FID" and "spectral" echoes of the kind illustrated in Fig. 1c were separated and processed individually. For each of the γB_1 strengths, a corresponding square-pulse CPMG experiment was also performed and the echoes resulting from this experiment were, following optimization, Fourier transformed. These are shown in Fig. 2c, color-coded for an easier comparison with their chirped-CPMG counterparts. As can be seen from this series, the improvement brought about by the use of swept pulses is not constant, and depends on the ratio between the available γB_1 and the width of the excited spectrum. When this ratio is small the excitation bandwidths that can be achieved from square and chirped-CPMG sequences are comparable; the sensitivity of the conventional experiment is then equal to or better than that of its chirped counterparts. As the RF power level increases, however, the sensitivity gains of the chirped-CPMG approach become noticeable. As can be appreciated from the line widths of the resulting spectral distributions, this is a reflection of the larger bandwidths that the chirped-CPMG sequence can excite and refocus, in comparison to the corresponding square-pulse CPMG sequence with the same maximal B_1.

Fig. 3 shows the full echo trains and with signal-to-noise comparisons resulting from co-adding all the odd echoes for the two experiments. These results confirm a significant increase in sensitivity upon employing the chirped-CPMG approach. As can be seen in the figure, where both sets of data are plotted in the same vertical gain and were acquired using equal gains, the signal-to-noise using matched filtering is improved by a factor of 10.0 in power units (or 3.16 in voltage units). Larger swept bandwidth experiments (not shown) revealed even larger enhancement factors.

Fig. 4 presents data obtained from a fringe-field low-frequency NMR. Although this setup was sited in a lab, it was akin to a well-logging tool in terms of magnetic field inhomogeneities and RF power levels. The probe and sample used in this experiment were placed in the fringe field of a 2 T horizontal magnet (Nalorac

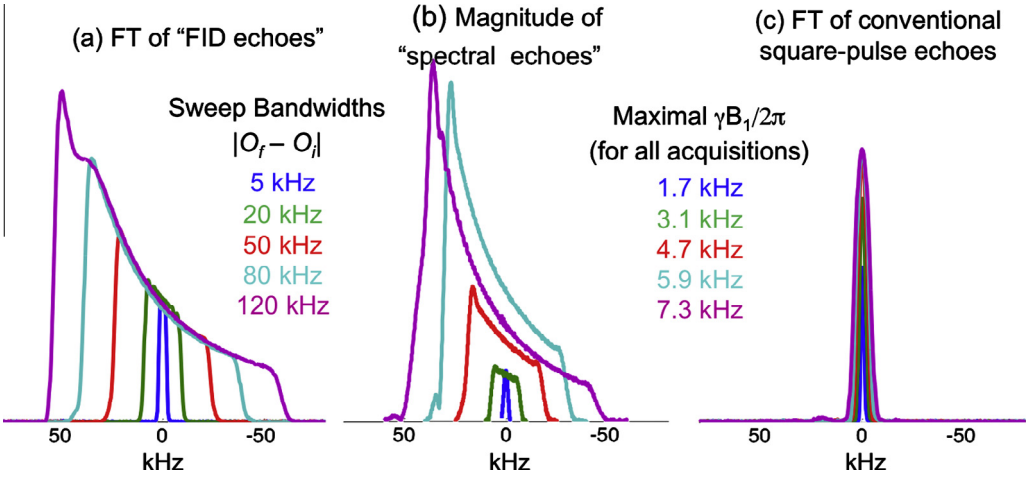

Fig. 2. Frequency-domain spectra obtained using a chirped-CPMG (a, b) and a conventional square-pulse CPMG (c) sequence. All spectra were recorded using four phase-cycled scans at equal receiving gains, using a 300 MHz NMR spectrometer and a sample whose line width had been artificially broadened to ca. 120 kHz (at half-height) using field gradients and off-center positioning. The maximum B_1 used for the chirped-CPMG was adjusted to the sweep bandwidth as coded by the various colors (second column). In (a) the odd echoes of a swept CPMG sequence were individually Fourier transformed (as were all echoes in (c)), whereas in (b) the time-domain signals are shown in absolute value. In this latter case the acquisition times t were converted into frequency offsets f according to Eq. (6). All spectra arise from summing all $N = 4$ (8 echoes) collected in the experiments prior to their processing. (For interpretation of the references to color in this figure legend, the reader is referred to the web version of this article.)

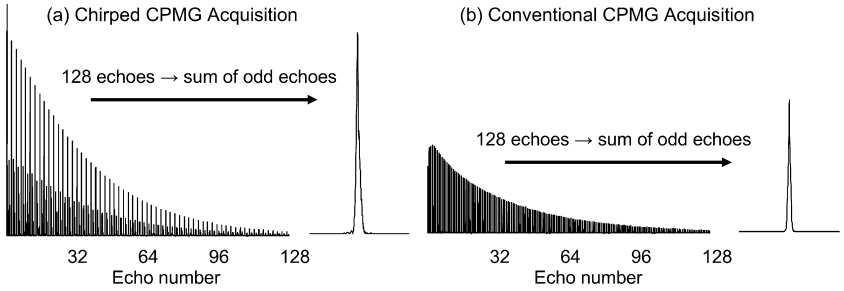

Fig. 3. CPMG echo trains and cumulative echo sums resulting from chirped (a) and conventional (b) CPMG experiments executed on a 300 MHz microimaging NMR for a sample of water doped with 1 g/L $CuSO_4$ whose linewidth had been artificially broadened to 100 kHz using field gradients. Data in (a) were collected using 20 kHz sweep ranges with a $\gamma B_1^{max} = 2\pi \times 2.9$ kHz for the swept π pulse; data in (b) were collected using the $\pi/2$ and π pulses of 85 and 145 μs long, respectively. All other parameters were the same as in Fig. 2.

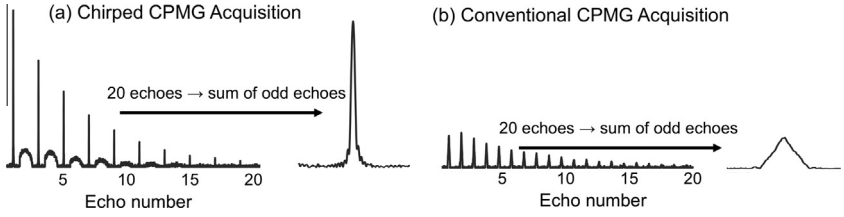

Fig. 4. Time-domain trains and cumulative echo sums collected on a Kea-based *ex situ* setup arising from chirped (a) and conventional (b) CPMG sequences. Data in (a) were collected using 100 kHz sweep ranges with a $\gamma B_1^{max} = 2\pi \times 5.0$ kHz for the swept π pulse; data in (b) were collected using $\pi/2$ and π pulses of 50 and 100 μs long, respectively. All other parameters were as in Fig. 2.

Cryogenics, Martinez, CA) leading to a Larmor frequency of 0.74 MHz with a gradient of 20 kHz/cm. The sample was approximately 4.5 cm and 5 cm in length and diameter, respectively, leading to ca. 100 kHz relevant linewidths. As can be seen in the figure, where both sets of data are plotted in the same vertical scale and were acquired using equal receiver gains, the signal-to-noise using matched filtering is improved by a factor of 4.71 in power units (or 2.17 in voltage units) in the chirped-CPMG sequence as compared to the standard CPMG.

To further highlight the differences in intensity and bandwidth afforded by the two CPMG methods, the asymptotic magnitude spectra arising from the time-domain data introduced in Figs. 3 and 4 are compared in Fig. 5. The larger bandwidths excited with the aid of the frequency sweeps is evident for both experimental setups. Fig. 5b also shows the close correspondence between the known profile of the cylindrical sample used in the fringe-field setup and the frequency profile afforded by the chirped-CPMG – a reflection of the constant receptivity that the used coil spanned over the sample volume. This panel also highlights the fact that under narrow-band excitation conditions the normal CPMG sequence can give a slightly superior local signal intensity (in this case at Offset ≈ 0), presumably reflecting its easier calibration of the RF pulse lengths.

5. Discussion and conclusions

The acquisition of faithful CPMG trains on inhomogeneously-broadened resonances is central to numerous areas in magnetic resonance, including solid state wideline NMR studies [10,19], MRI [20,21] in the presence of field gradients, and well-logging applications [4,22,23]. In the latter two cases, B_1 inhomogeneities

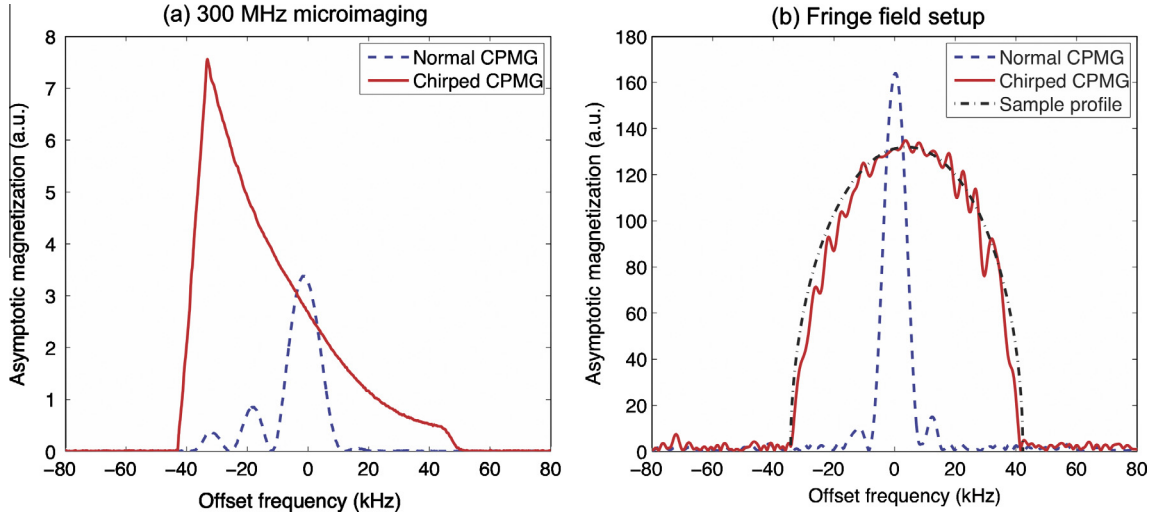

Fig. 5. Asymptotic magnitude spectra of the conventional and chirped-CPMG sequences measured in (a) a high-field vertical microimaging system, and (b) a low-field fringe-field setup. Only the odd echoes were back-extrapolated to zero echo times, in the derivation of all plots.

further complicate the unambiguousness, sensitivity and overall usefulness of the experiment. Given these penalties, extensive efforts have been invested to overcome these complications; in the well-logging case these have included the use of composite pulses [24,25], optimal control algorithms [26], and trains incorporating imperfection-matched nutation axes [27]. Here we show that frequency-swept pulses can also be successfully employed as a part of these improvements, within the CPMG family of pulse sequences. In their simplest implementation, the resulting experiments will lead to an alternating series of conventional ("FID") and "spectral" echoes, which although of different appearance carry the same information and can be combined into a single all-encompassing spectrum. Moreover, although not implemented in the present study, it can be shown that the use of super-resolution post-acquisition processing procedures will endow the spectral echoes with sensitivities that are similar to those of their time-domain "FID" counterparts [28]. It follows from this that for a given number of CPMG echoes, the increase in sensitivity provided by this approach will be in direct proportion to the wider range of frequencies that a swept-pulse sequence will address for a maximal γB_1 vis-à-vis its square-pulse counterpart. The critical parameter under the experimentalist's control in this kind of experiment thus becomes the chirped pulse's Time-Bandwidth Product (TBP). As this parameter is usually $\geqslant 20$ and since the number of spins contributing to a signal grows as $\sqrt{TBP_{chirp}}$, fourfold or higher increases in the addressable bandwidths are thus expected upon applying these experiments. The signal enhancements arising from these predictions are in principle larger than most of the remaining *ex situ* liquids NMR alternatives mentioned earlier, and can be carried out with only a slight modification of the conventional CPMG into a simple and robust swept-pulse counterpart. With these predictions as background the experimental section of this work focused on exploring these features using WURST-shaped frequency-swept pulses, on high- and low-field NMR scenarios characterized by large B_0 field inhomogeneities. The ensuing results relied on these intrinsic line broadenings to demonstrate a consistent increase in the bandwidths of the excited/refocused spins: as predicted, even moderate RF fields yielded swept inversion profiles that exceeded by many-fold the square-wave counterparts recorded with the same γB_1's.

In the interest of completeness, some disadvantages of the chirped CPMG sequence should also be highlighted. As the frequency-swept pulses are longer than corresponding hard pulses, this necessitates correspondingly longer echo times than a standard CPMG sequence. This means that (i) samples with extremely short T_2 values are not amenable to measurement using this technique; (ii) standard CPMGs can be collected with a higher echo duty cycle, which allows more echoes to be collected within a given acquisition time for increased signal-to-noise and reduced sensitivity to molecular diffusion; and (iii) the average power and total deposited energy requirements over the course of the experiment are increased in the chirped-CPMG sequence as compared to the standard sequence – even at equal peak power levels – and heating effects can be expected to be more significant in chirped-CPMG than with the standard CPMG sequence.

It is of interest to highlight the different diffusion sensitivities expected by the conventional vis-à-vis the chirped-CPMG sequences. For example, the slower refocusing associated to the chirped-CPMG experiment should lead to different diffusion decays than in a conventional CPMG counterpart. While this issue is still being studied, it is conceivable that the different behaviors expected for the two sequences might be exploited to get insight into the fluid's diffusivity; for instance, by comparing the effective transverse decay constants afforded by the two experiments. It appears likely that, in addition to the significant decreases in experimental time made possible by increased SNR, the implementation of chirped-CPMG sequences could simultaneously reveal details about sample porosity and pore size distributions, from their line shapes. While a full analysis of this effect has not been completed, it is interesting to point out its potential to discern the actual diffusivity/viscosity characteristics of the examined fluid – a central need of well-logging experiments for distinguishing water from oil-rich liquids [29,30].

Acknowledgments

We thank Joseph Chen for detailed characterization of the fringe-field system and for programming WURST pulses, as well as to Eddy Solomon for valuable discussions. Financial support from the Israel Science Foundation (Grant ISF 795/13), EuroMagNet's EU Contract #228043, a Helen and Kimmel Award for Innovative Investigation, and the generosity of the Perlman Family Foundation, are gratefully acknowledged.

References

[1] R.L. Kleinberg, J.A. Jackson, Concepts Magn. Reson. 13 (2001) 340–342.
[2] R.L. Kleinberg, Concepts Magn. Reson. 13 (2001) 342–343.
[3] R. Heidler, H.N. Bachman, Y. Johansen, AIP Conf. Proc. 1081 (2008) 95–98.
[4] G. Goelman, M.G. Prammer, J. Magn. Reson., A 113 (1995) 11–18.
[5] H.Y. Carr, E.M. Purcell, Phys. Rev. 94 (1954) 630–638.
[6] S. Meiboom, D. Gill, Rev. Sci. Instrum. 29 (1958) 688–691.
[7] R. Bhattacharyya, L. Frydman, J. Chem. Phys. 127 (2007) 194503.
[8] J.M. Böhlen, M. Rey, G. Bodenhausen, J. Magn. Reson. 84 (1989) 191–197.
[9] V.L. Ermakov, J.M. Böhlen, G. Bodenhausen, J. Magn. Reson., A 103 (1993) 226–229.
[10] L.A. O'Dell, R.W. Schurko, Chem. Phys. Lett. 464 (2008) 97–102.
[11] A.W. MacGregor, L.A. O'Dell, R.W. Schurko, J. Magn. Reson. 208 (2011) 103–113.
[12] A. Tal, L. Frydman, J. Magn. Reson. 182 (2006) 179–194.
[13] R. Freeman, Spin Choreography, Oxford University Press, 1998.
[14] D. Kunz, Magn. Reson. Med. 3 (1986) 377–384.
[15] Y. Shrot, L. Frydman, J. Magn. Reson. 172 (2005) 179–190.
[16] E. Kupce, R. Freeman, J. Magn. Reson., A 115 (1995) 273–276.
[17] S. Utsuzawa, S. Mandal, Y.Q. Song, J. Magn. Reson. 216 (2012) 128–133.
[18] S. Mandal, S. Utsuzawa, Y.Q. Song, Microporous Mesoporous Mater. 178 (2013) 5355–5357.
[19] F.H. Larsen, J. Skibsted, H.J. Jakobsen, N.Chr. Nielsen, J. Am. Chem. Soc. 122 (2000) 7080–7086.
[20] K. Oshio, D.A. Feinberg, Magn. Reson. Med. 20 (1991) 344–349.
[21] A.A. Maudsley, J. Magn. Reson. 38 (1997) 527–533.
[22] T.B. Benson, P.J. McDonald, J. Magn. Reson., B 109 (1995) 314–317.
[23] M.D. Hürlimann, D.D. Griffin, J. Magn. Reson. 143 (2000) 120–135.
[24] M.D. Hürlimann, J. Magn. Reson. 152 (2001) 109–123.
[25] V.D.M. Koroleva, S. Mandal, Y.Q. Song, M.D. Hürlimann, J. Magn. Reson. 230 (2013) 64–75.
[26] T.W. Borneman, M.D. Hürlimann, D.G. Cory, J. Magn. Reson. 207 (2010) 220–233.
[27] S. Mandal, V.D.M. Koroleva, T.W. Borneman, Y.Q. Song, M.D. Hürlimann, J. Magn. Reson. 237 (2013) 1–10.
[28] N. Ben-Eliezer, Y. Shrot, L. Frydman, D.K. Sodickson, Magn. Reson. Med. (2014). http://dx.doi.org/10.1002/mrm.24954 (in press).
[29] P.J. McDonald, Prog. Nucl. Magn. Reson. Spectrosc. 30 (1997) 69–99.
[30] M.D. Hürlimann, J. Magn. Reson. 148 (2001) 367–378.